Supplementary materials

Molecularly imprinted polymer on cotton materials as substrates combined with smartphone-based image and distance-based analysis of Cu (II) in water samples

N. Thongkon*[a], Phakamas Maisom[a], Orawan Taewcharoen[a], Wannaree Kamsomjit[a], Supacha Nilsuwan[a], Nattakul Saejan[a] and S. Somrak[a],

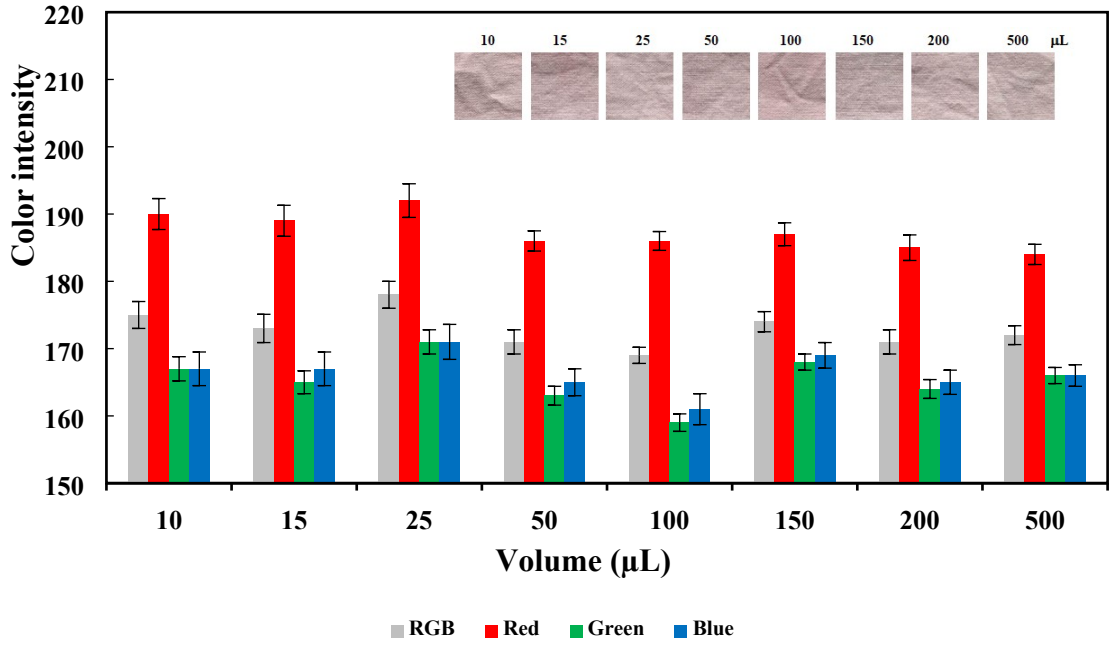

Fig. S1 Comparison of color intensity after varying the volume of TEOS for the CF-MIP/PAR-Cu (II).

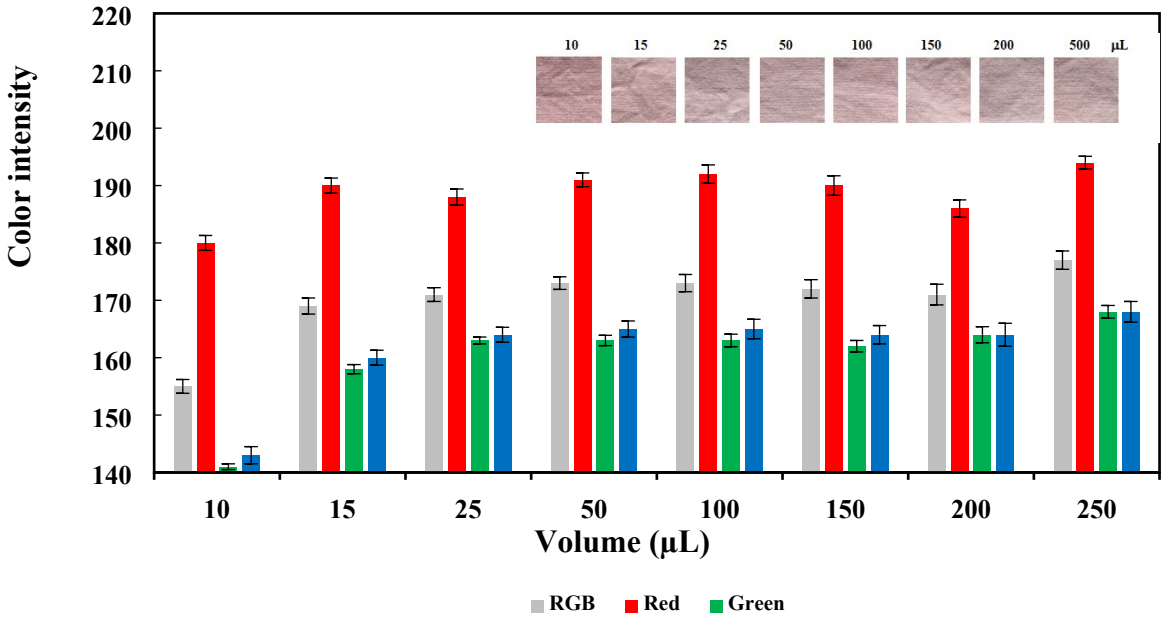

Fig. S2 Comparison of color intensity after varying the volume of APTES for the CF-MIP/PAR-Cu (II).

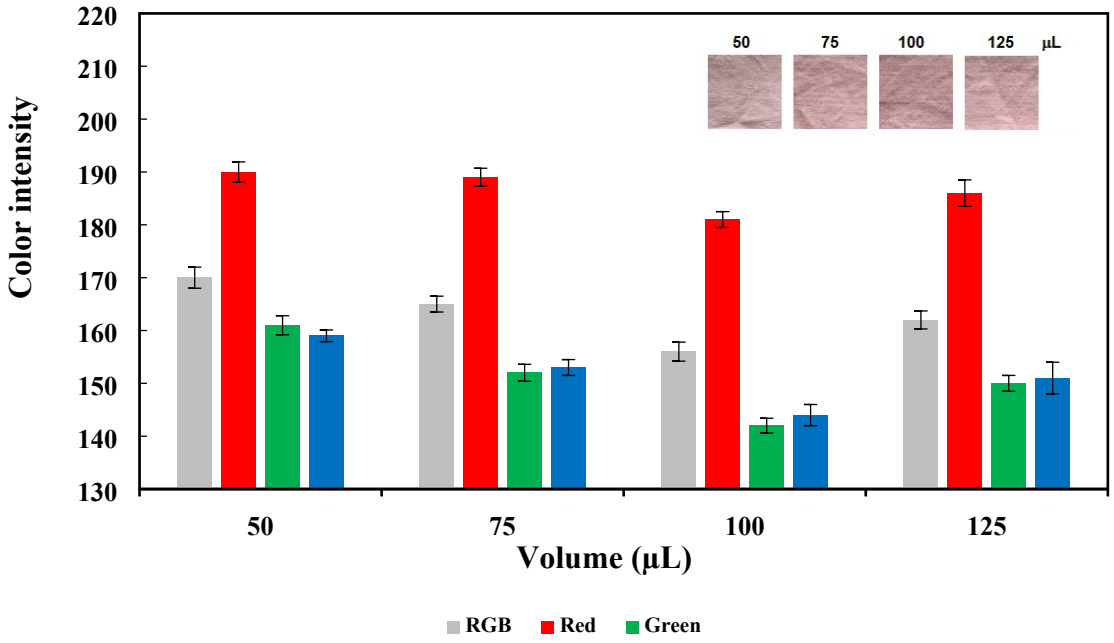

Fig. S3 Comparison of color intensity after varying the volume of NH_3 for the CF-MIP/PAR-Cu (II).

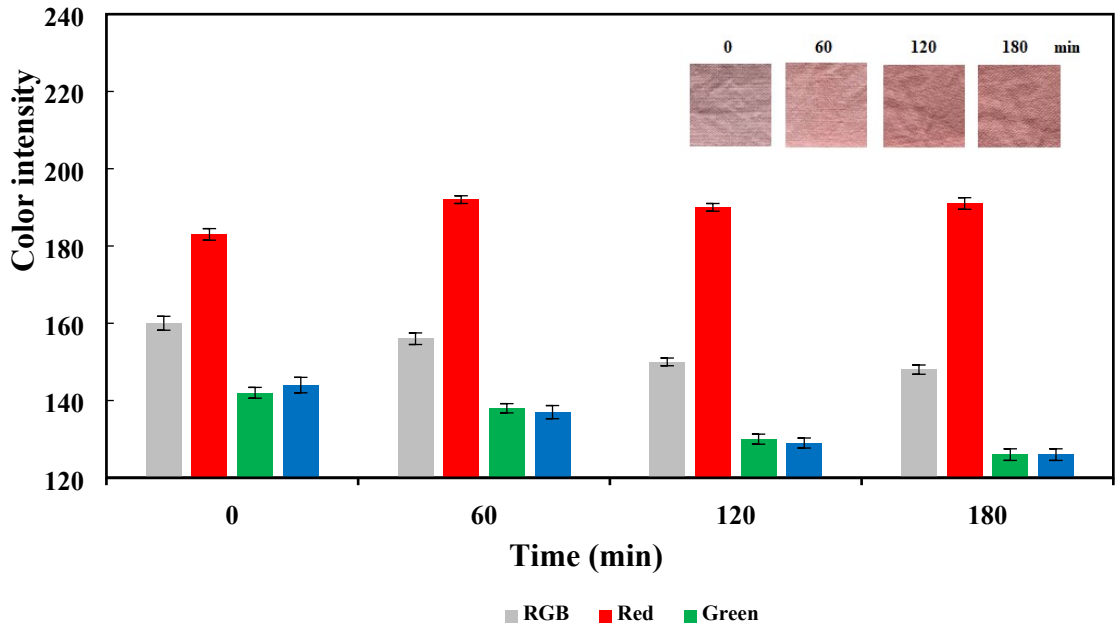

Fig. S4 Comparison of color intensity after varying reaction time after using vortex (10 min) for the CF-MIP/PAR-Cu (II).

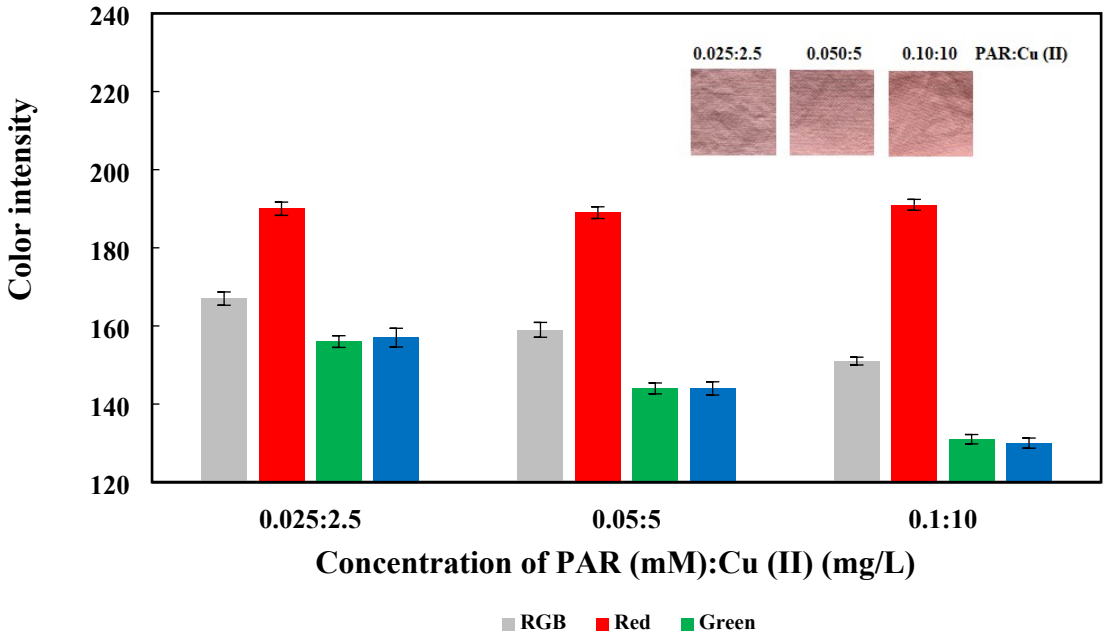

Fig. S5 Comparison of color intensity after varying the concentration of PAR and Cu (II) for the CF-MIP/PAR-Cu (II).

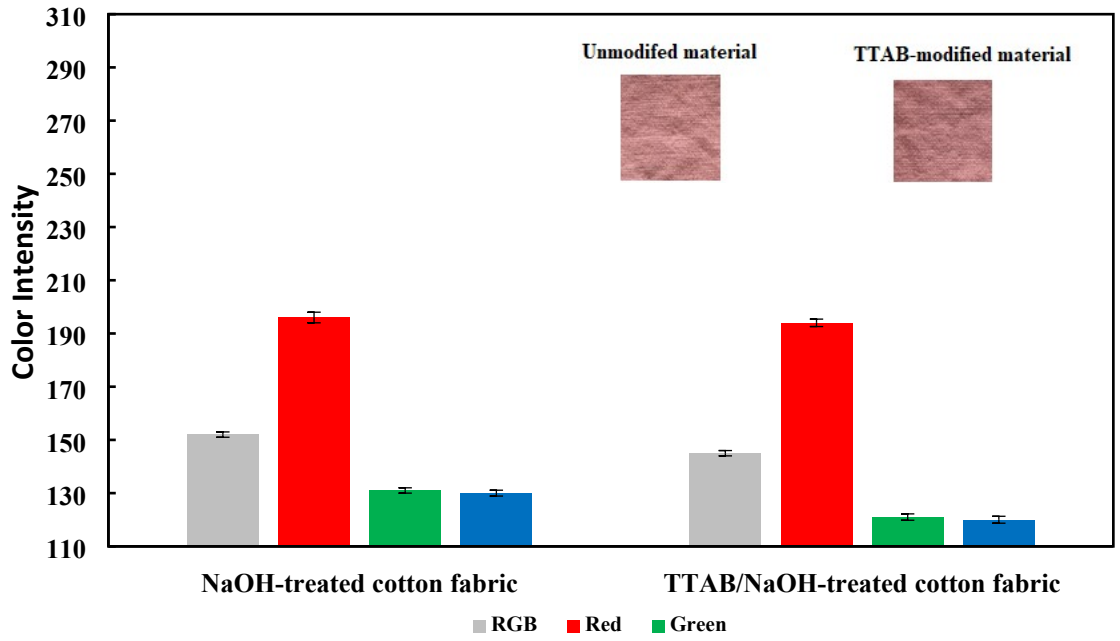

Fig. S6 Comparison of color intensity between NaOH-treated cotton fabric and TTAB/NaOH-treated cotton fabric for the MIP/PAR-Cu (II) modified materials.

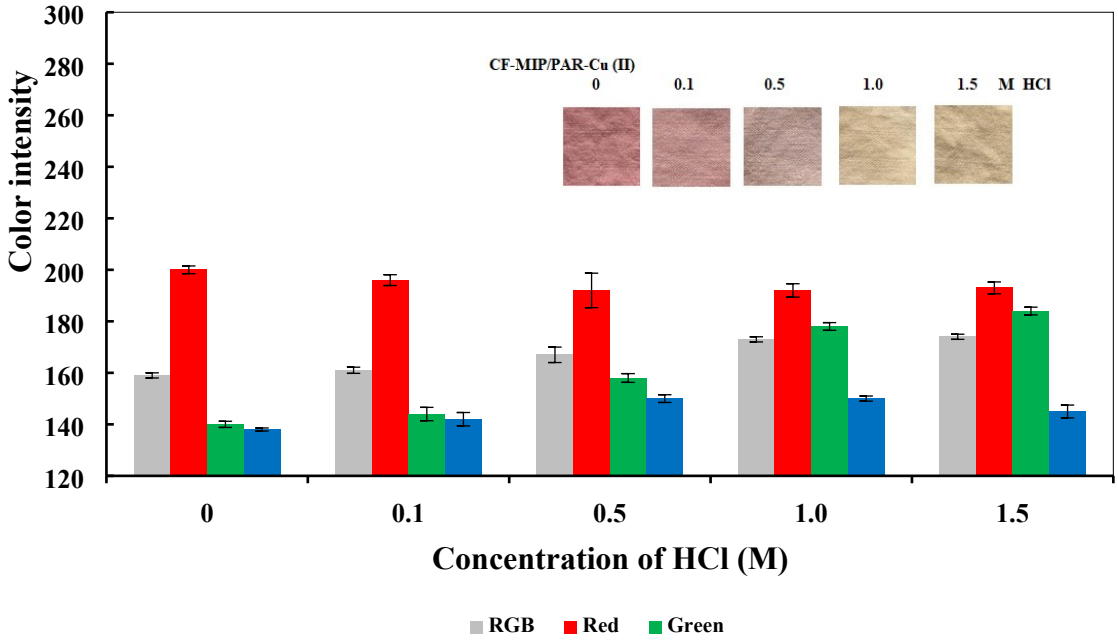

Fig. S7 Comparison of color intensity after varying the concentration of HCl for extracting Cu (II) ions from the CF-MIP/PAR-Cu (II) for 5 min.

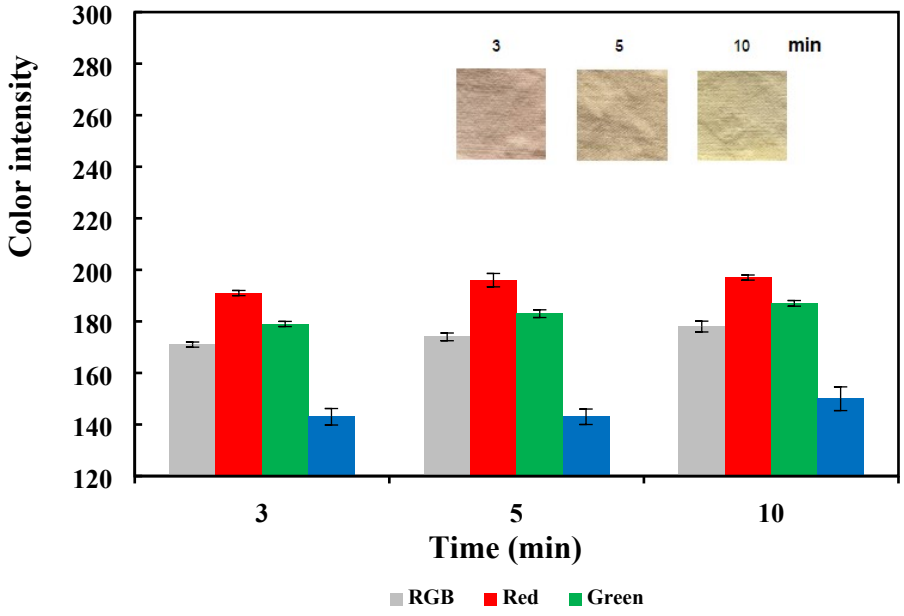

Fig. S8 Comparison of color intensity after using 1.5 M HCl by varying the extraction time for extracting Cu (II) ions from the CF-MIP/PAR-Cu (II).

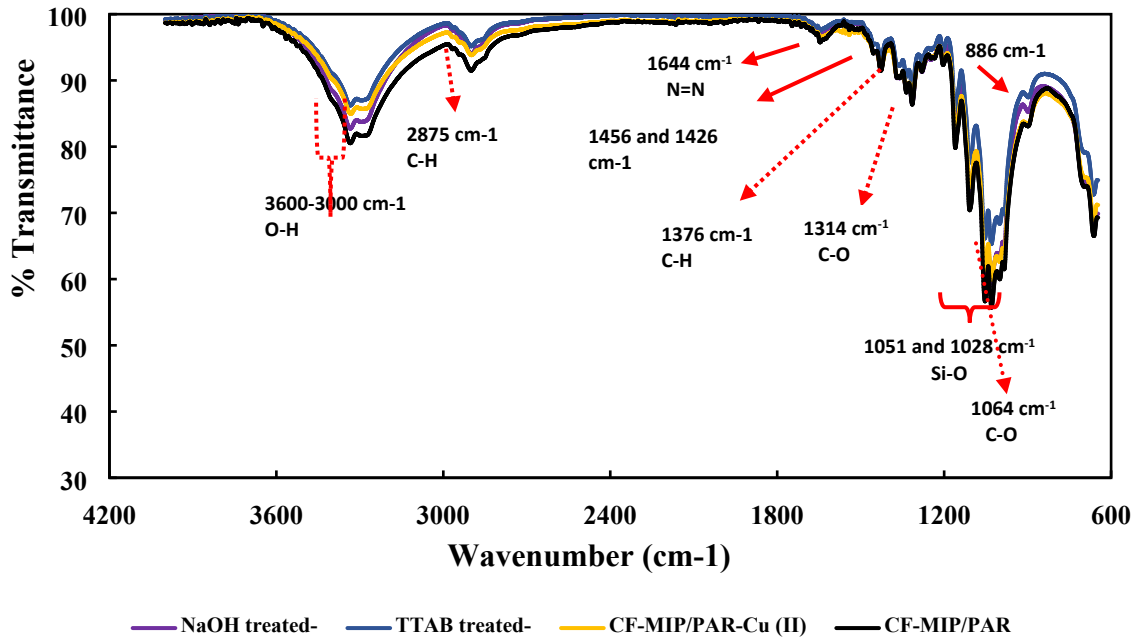

Fig. S9 ATR-FTIR spectrum of a) NaOH-treated cotton fabric, b) TTAB/NaOH-treated cotton fabric (CF), c) CF-MIP/PAR-Cu (II), and d) CF-MIP/PAR.

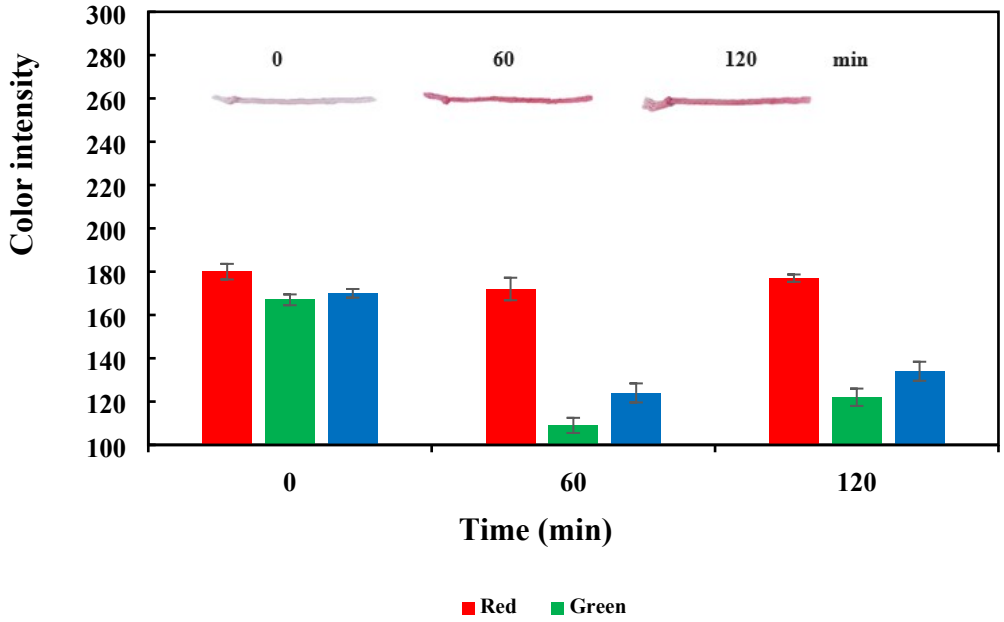

Fig. S10 Comparison of color intensity after varying reaction time and using vortex (10 min) for the CT-MIP/PAR-Cu (II) with the single-channel type.

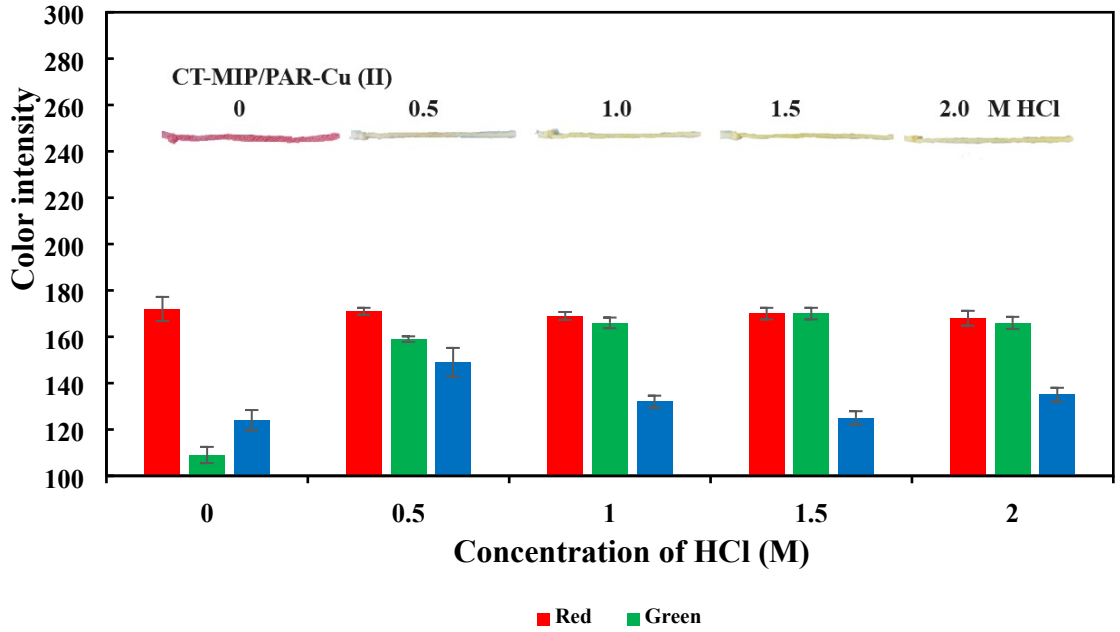

Fig. S11 Comparison of color intensity after varying the concentration of HCl for extracting Cu (II) ions from the CT-MIP/PAR-Cu (II) with the single-channel type for 5 min.

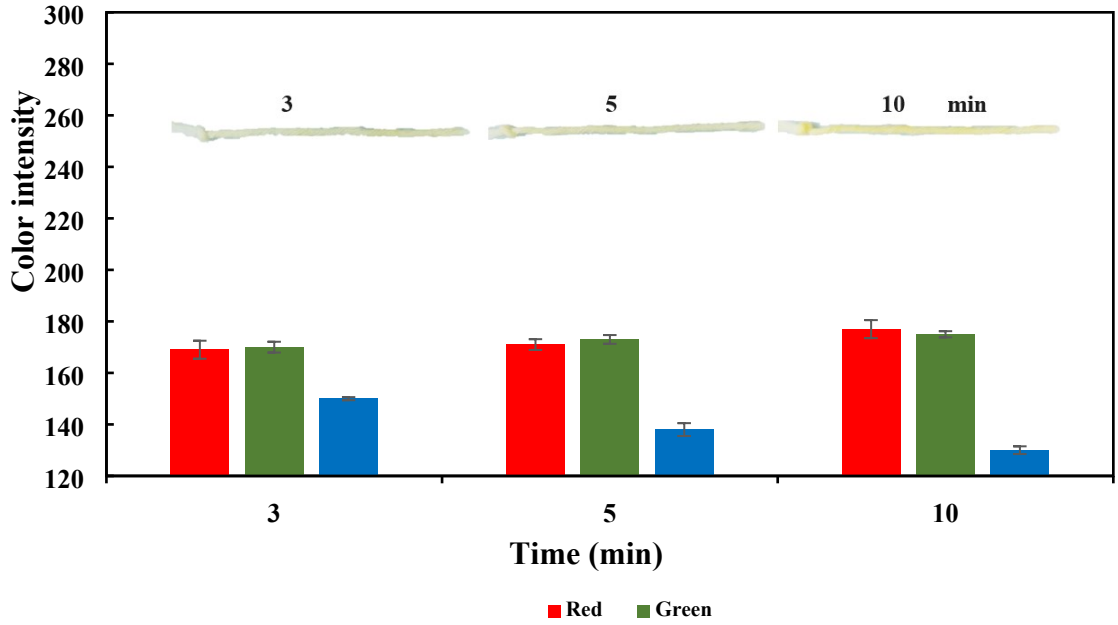

Fig. S12 Comparison of color intensity after using 1.5 M HCl by varying the extraction time for extracting Cu (II) ions from the CT-MIP/PAR-Cu (II) with the single-channel type.

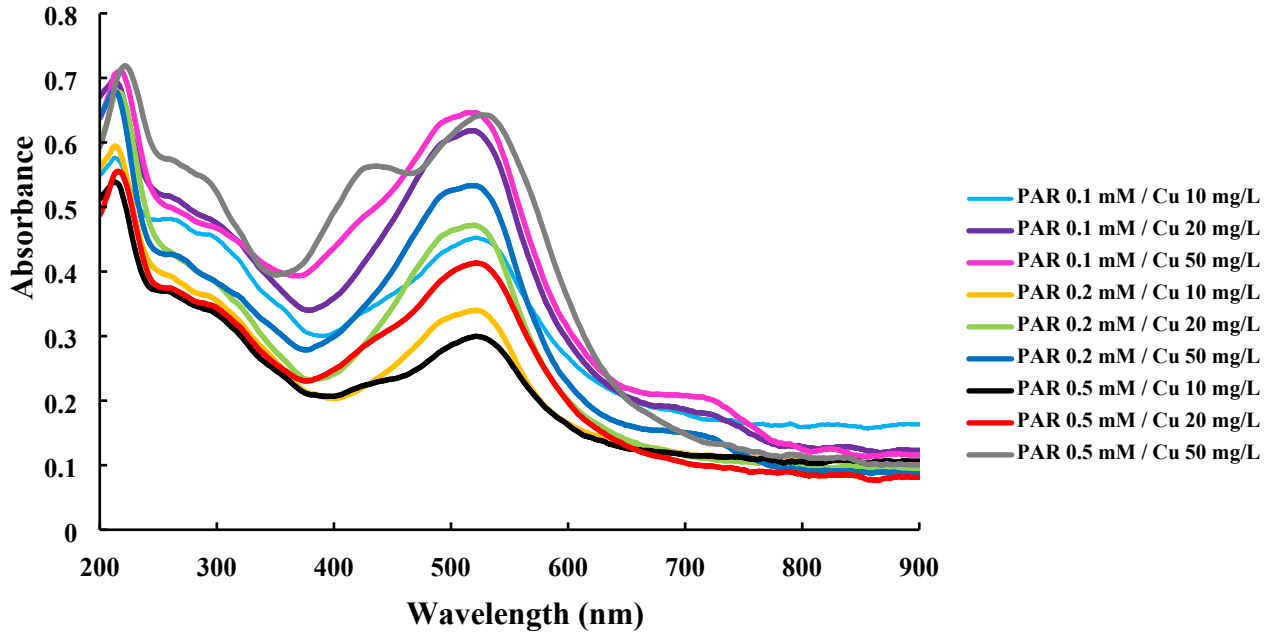

Fig. S13 UV/Visible absorption spectrum of the CT-MIP/PAR-Cu (II) from using different concentration of PAR and Cu (II) as template molecules.

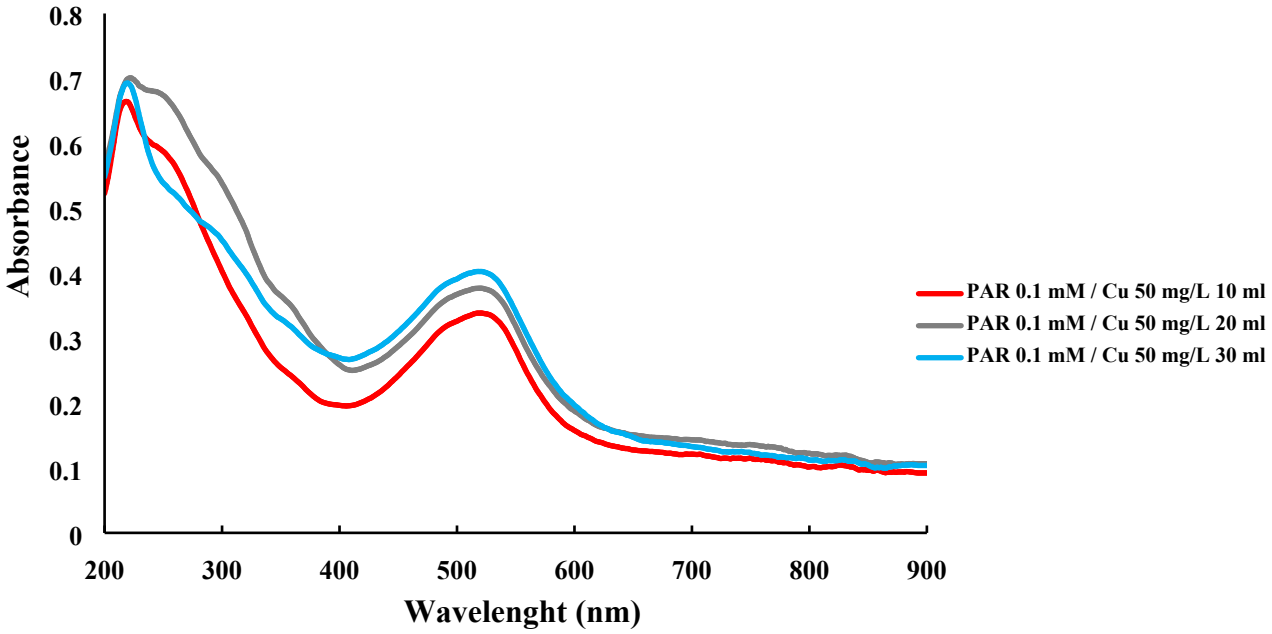

Fig. S14 UV/Visible absorption spectrum of the four-channel CT-MIP/PAR-Cu (II) from using 0.1mM PAR/50 mg/L Cu (II) at different solution volume.

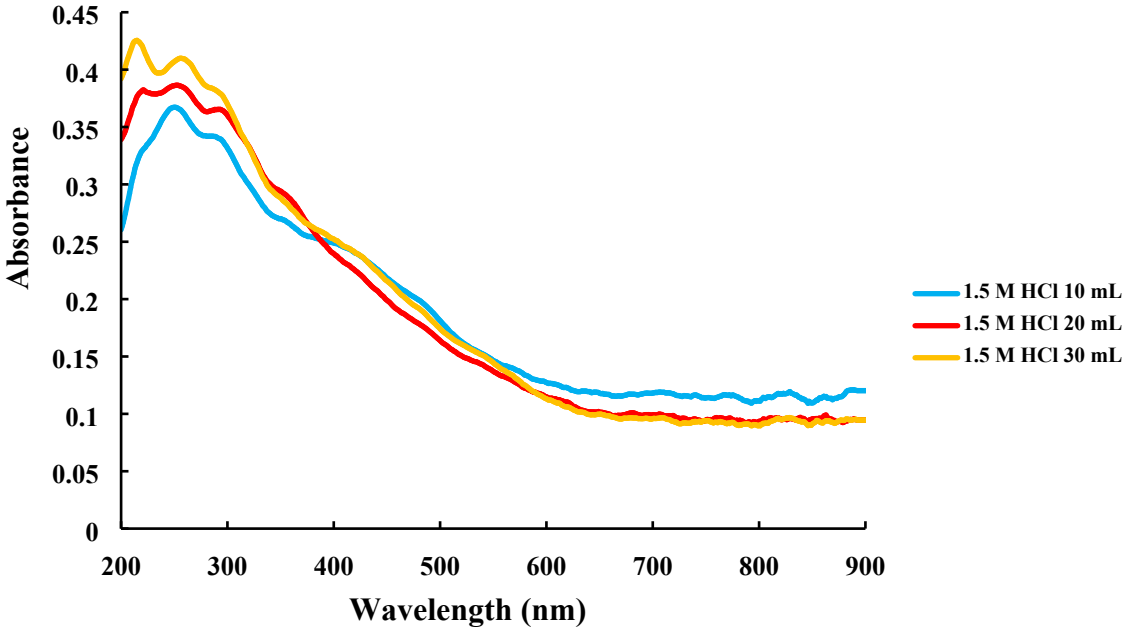

Fig. S15 UV/Visible absorption spectrum of the four-channel CT-MIP/PAR from using 1.5M HCl at different volume for extraction.

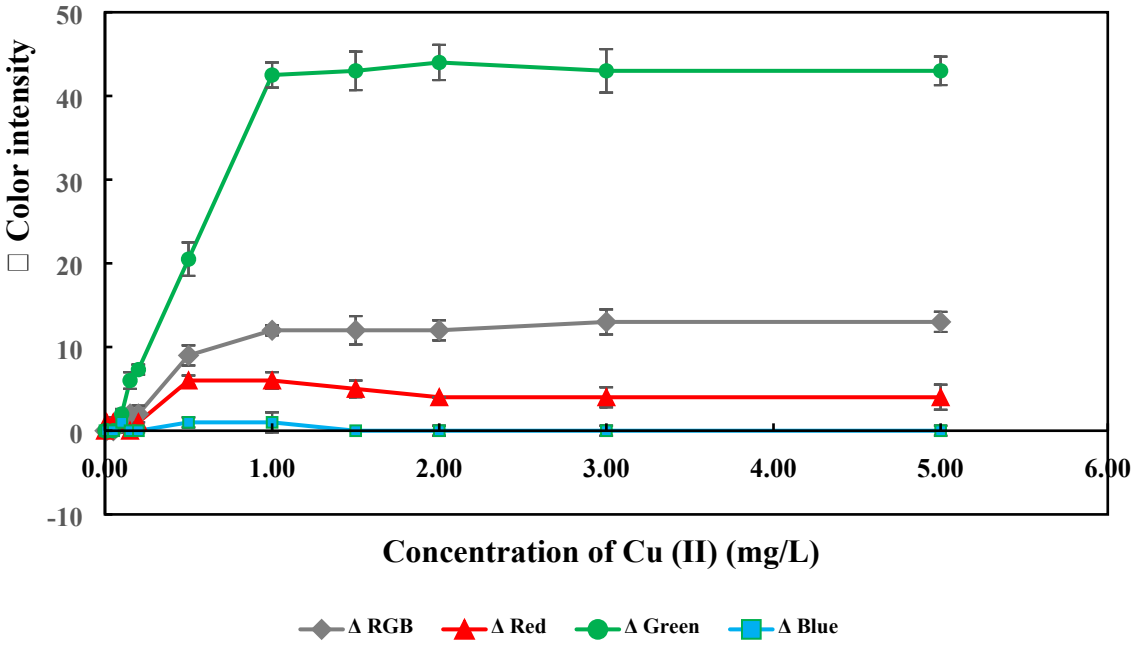

(A)

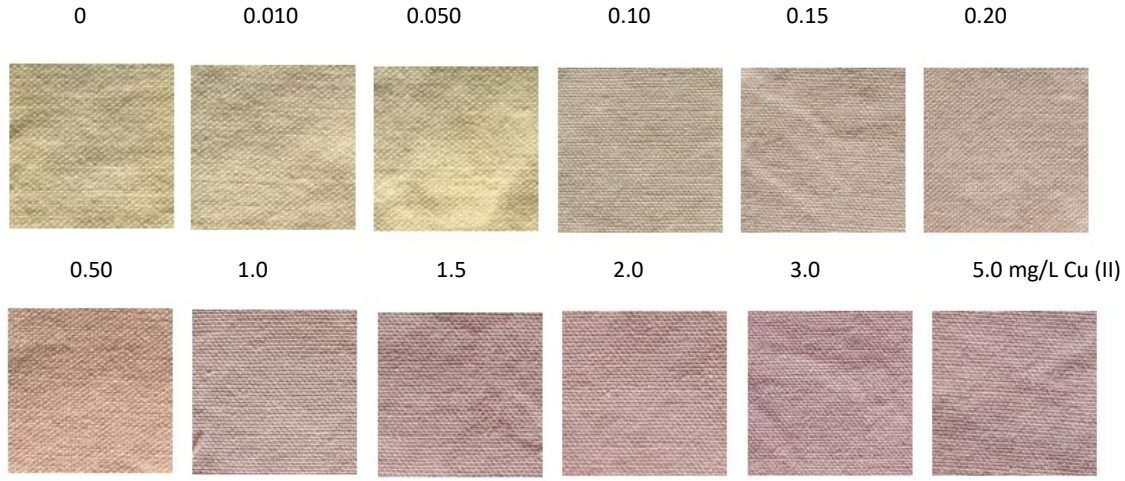

(B)

Fig. S16 (A) Graph plotted between Δ color intensity vs. concentration of Cu (II), and (B) Digital images of the CF-MIP/PAR from detection of various concentrations.

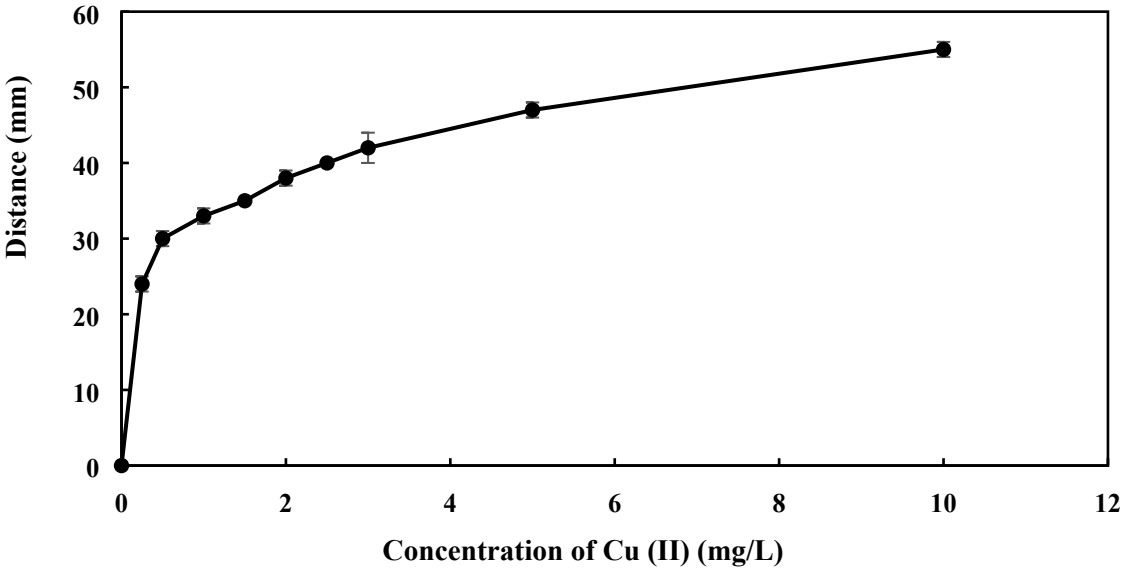

Fig. S17 Graph plotted between distance vs. concentration of Cu (II) of the single-channel CT-MIP/PAR.

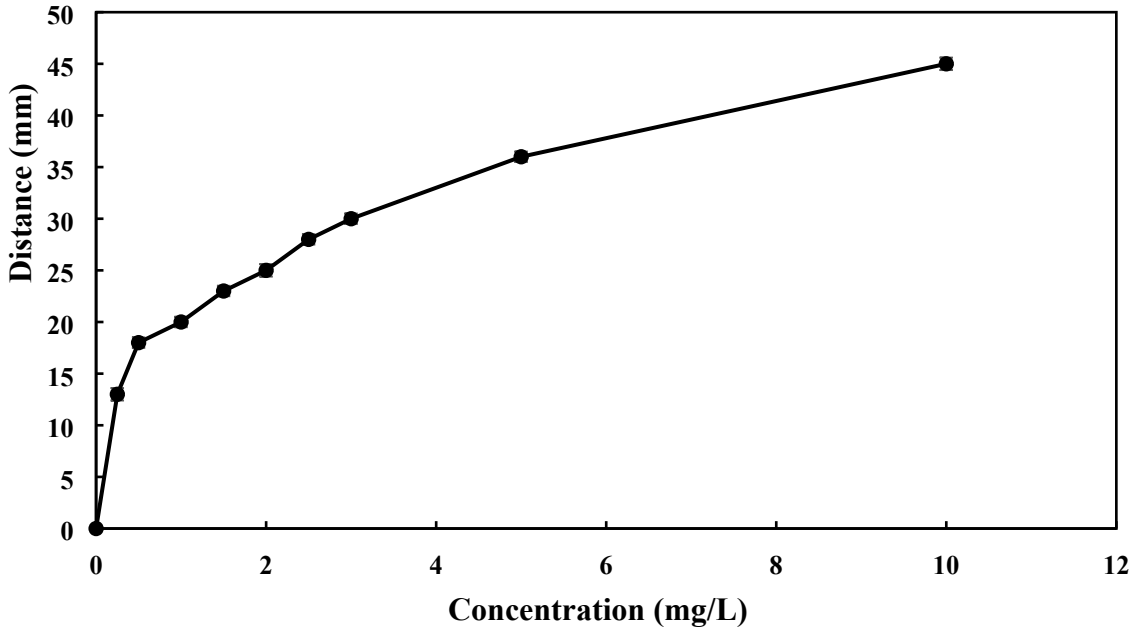

Fig. S18 Graph plotted between distance vs. concentration of Cu (II) of the four-channel CT MIP/PAR.

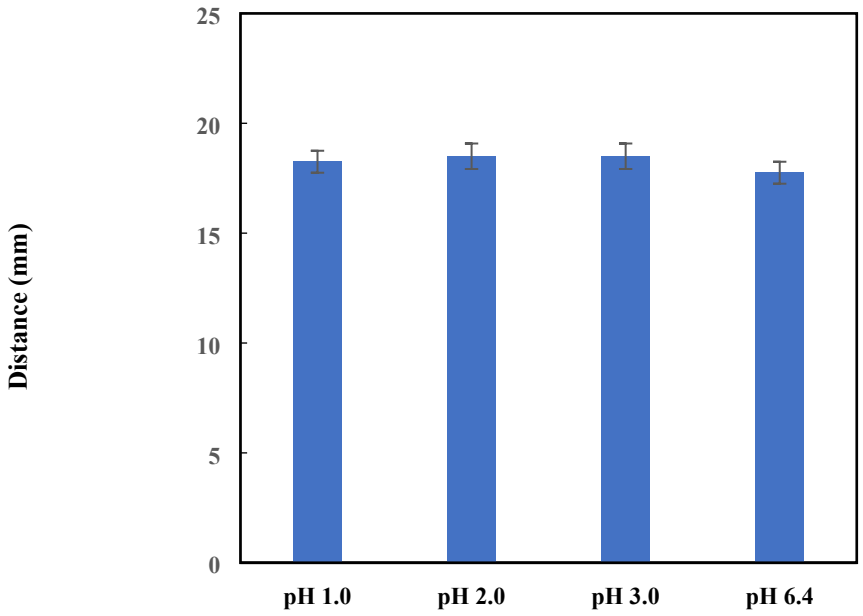

(A)

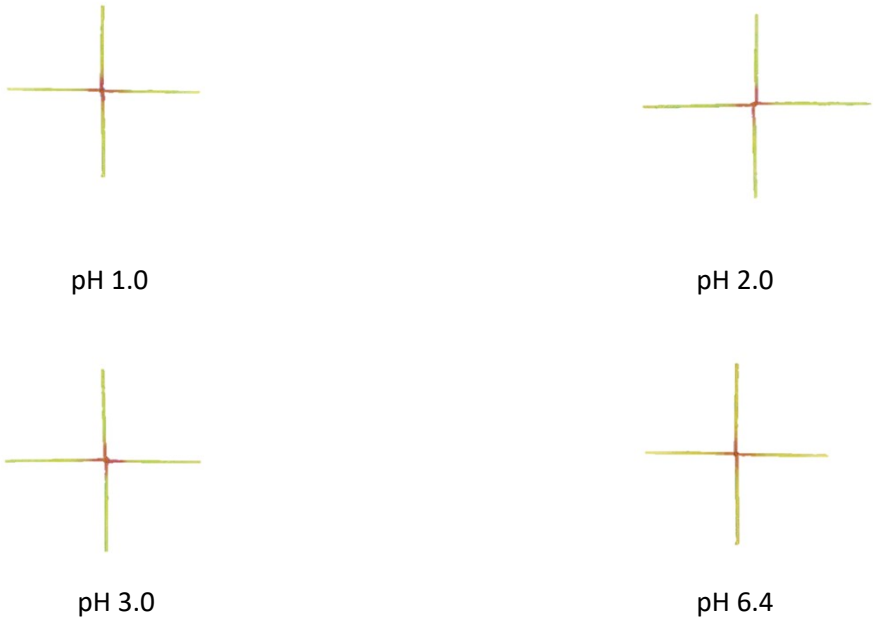

(B)

Fig. S19 (A) The effect of pH on the distance measurement from the detection of Cu (II) at a concentration of 0.5 mg/L and the digital images using the four-channel CT-MIP/PAR.